Transition between coupled-resonator-induced transparency and absorption

Shu-Ting Guo, Yu-Hong Zhang, Liu-Le Wu, Ming-Yong Ye,* and Xiu-Min Lin
Fujian Provincial Key Laboratory of Quantum Manipulation and New Energy Materials, College of Physics and Energy, Fujian Normal University, Fuzhou 350117, China
and Fujian Provincial Collaborative Innovation Center for Advanced High-Field Superconducting Materials and Engineering, Fuzhou 350117, China

(Received 18 August 2020; revised 16 February 2021; accepted 1 March 2021; published 17 March 2021)

Electromagnetically induced transparency and absorption in atomic systems have applications such as slow-light generation. Coupled-resonator-induced transparency (CRIT) and absorption (CRIA) are the optical analogy to them. Here we theoretically and experimentally study CRIT and CRIA in two directly coupled whispering-gallery-mode microresonators. The theoretical results give conditions for observing CRIT and CRIA, and predict that a transition between them will happen if we change the coupling strength between the two microresonators or the coupling strength between the fiber taper and the first microresonator. The experimental results demonstrate the transitions between CRIT and CRIA using a microsphere coupled to a sausagelike microresonator. The obtained results give some guidelines to observe CRIT and CRIA.

DOI: 10.1103/PhysRevA.103.033510

I. INTRODUCTION

Electromagnetically induced transparency (EIT) in atomic systems, relying on quantum interference to diminish absorption, has found extensive optical applications [1]. In recent years, there has been much interest in observing all-optical analogues of EIT in optical resonators [2,3]. The related works include observing an EIT-like phenomenon in a single optical resonator [4–8], observing an EIT-like phenomenon in two coupled optical resonators [9–13], and observing optomechanically induced transparency [14–17]. It is one advantage that an EIT-like phenomenon in optical resonators can be observed at room temperature, which is very important for its future wide applications.

A whispering-gallery-mode (WGM) microresonator, such as a silica microsphere and microdisk, is a kind of optical resonator that can support optical modes with ultra-high-quality factors and small mode volumes and has wide applications [18–20]. Two coupled WGM microresonators provide a very good platform to study EIT-like phenomena in which several system parameters related to EIT can be adjusted independently. The EIT-like phenomenon in two coupled resonators is also called coupled-resonator-induced transparency (CRIT) [9,21], which is typically manifested by a narrow peak in the background of a broad transmission dip. In addition to CRIT, there is also the coupled-resonator-induced absorption (CRIA) phenomenon [9], which shows a narrow dip in the background of a broad transmission dip. The application of CRIT in slow light has been experimentally demonstrated in two coupled microspheres [10]. Multiple CRIT and CRIA are observed in two coupled WGM microresonators [22]. Very recently, CRIT and CRIA have been observed in two indirectly coupled WGM microresonators with exceptional point [23]. Additionally, WGM microresonators coupled to a waveguide can be used to discuss novel optical transport and correlation phenomena with quantum coherence [24–26].

In this paper, CRIT and CRIA in two directly coupled WGM microresonators are studied theoretically and experimentally. In the theory study, conditions for observing CRIT and CRIA are obtained and we discuss how to achieve a transition between CRIT and CRIA. In the experimental study, the transmission spectra of the coupled system of a microsphere and a sausagelike microresonator (SLM) [27] are measured under different conditions. Our results demonstrate clear observations of transitions between CRIT and CRIA, the related Fano resonance [28–33], and Autler-Townes splitting (ATS) [12].

II. THEORETICAL MODEL AND ITS TRANSMISSION SPECTRUM

The considered theoretical model is shown in Fig. 1. Microresonator μR_1 supports a WGM of resonant angular frequency ω_1 with an intrinsic loss rate κ_{o1}, which is coupled to a fiber taper with a coupling strength κ_{e1}. In the following, the parameter $\kappa_1 = \kappa_{o1} + \kappa_{e1}$ will be used to denote its total loss rate. Microresonator μR_2 supports a WGM of resonant angular frequency ω_2 with a total loss rate κ_2 that is equal to its intrinsic loss rate as μR_2 has no coupling with the fiber taper. The two microresonators have a coupling with strength g. The dynamical equations governing the fields of two WGMs are

$$\frac{dE_1(t)}{dt} = (-i\omega_1 - \kappa_1)E_1(t) - igE_2(t) + \sqrt{2\kappa_{e1}}E_{\rm in}(t), \quad (1)$$

$$\frac{dE_2(t)}{dt} = (-i\omega_2 - \kappa_2)E_2(t) - igE_1(t), \quad (2)$$

where $E_1(t)$ and $E_2(t)$ represent the fields of the WGMs in μR_1 and μR_2, respectively. The output field from the fiber taper is $E_{\rm out}(t)$, whose relation to the input field $E_{\rm in}(t)$

*Corresponding author: myye@fjnu.edu.cn

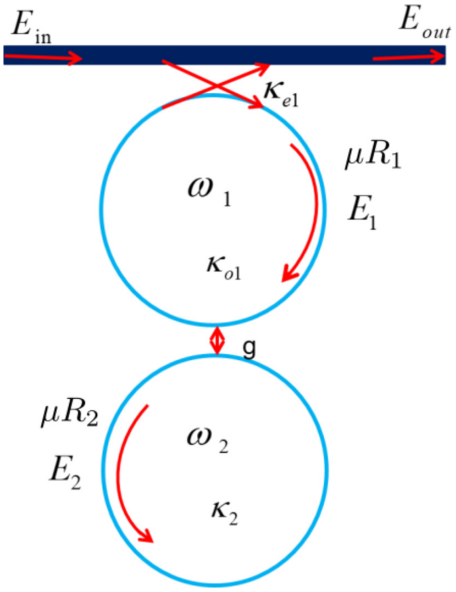

FIG. 1. A schematic diagram of two coupled WGM microresonators. The above microresonator is coupled to a fiber taper.

is given by

$$E_{\text{out}}(t) = -E_{\text{in}}(t) + \sqrt{2\kappa_{e1}}E_1(t). \tag{3}$$

The normalized transmission of the system is defined as

$$T = \left|\frac{E_{\text{out}}(t)}{E_{\text{in}}(t)}\right|^2, \tag{4}$$

which is usually dependent on the time t. In the case that the input field $E_{\text{in}}(t)$ has the angular frequency ω, the time-dependent part of T will decay exponentially and, finally, T will go to its stationary value,

$$T = \left|\frac{[\kappa_{e1} - \kappa_{o1} + i(\Delta\omega - \delta_{12})](-i\Delta\omega + \kappa_2) - g^2}{[\kappa_{e1} + \kappa_{o1} - i(\Delta\omega - \delta_{12})](-i\Delta\omega + \kappa_2) + g^2}\right|^2, \tag{5}$$

where $\Delta\omega = \omega - \omega_2$ and $\delta_{12} = \omega_1 - \omega_2$. The above stationary normalized transmission T describes the transmission spectrum of the theoretical model, which will be used to fit our experimental observation.

III. CONDITIONS FOR OBSERVING CRIT AND CRIA

Assume that two WGMs have the same angular frequency, i.e., $\delta_{12} = \omega_1 - \omega_2 = 0$. In this case, the normalized transmission $T|_{\delta_{12}=0}$ as a function of the angular frequency detuning $\Delta\omega$ is an axisymmetric function because it is an expression of $(\Delta\omega)^2$. The transmission at the symmetry axis (resonance input) is

$$T\big|_{\delta_{12}=0,\Delta\omega=0} = \left|1 - \frac{2\kappa_{e1}\kappa_2}{(\kappa_{e1} + \kappa_{o1})\kappa_2 + g^2}\right|^2. \tag{6}$$

When μR_2 is not coupled to μR_1, the function shape of T will be a Lorentzian dip and the transmission at the symmetry axis (resonance input) is

$$T\big|_{\delta_{12}=0,\Delta\omega=0,g=0} = \left|1 - \frac{2\kappa_{e1}}{\kappa_{e1} + \kappa_{o1}}\right|^2. \tag{7}$$

Define

$$D = T\big|_{\delta_{12}=0,\Delta\omega=0} - T\big|_{\delta_{12}=0,\Delta\omega=0,g=0}. \tag{8}$$

If $D > 0$, the coupling of μR_2 to μR_1 increases the transition at the resonance input. If $D < 0$, the coupling of μR_2 to μR_1 decreases the transition at the resonance input. Therefore, when $D > 0$ ($D < 0$), we will say there is a CRIT (CRIA) phenomenon. It can be found that

$$D = \frac{4g^2\kappa_{e1}\left(\kappa_{o1}g^2 + \kappa_{o1}^2\kappa_2 - \kappa_{e1}^2\kappa_2\right)}{[(\kappa_{e1} + \kappa_{o1})\kappa_2 + g^2]^2(\kappa_{e1} + \kappa_{o1})^2}. \tag{9}$$

Therefore, the condition for observing CRIT is

$$\kappa_{o1}g^2 + \left(\kappa_{o1}^2 - \kappa_{e1}^2\right)\kappa_2 > 0, \tag{10}$$

and the condition for observing CRIA is

$$\kappa_{o1}g^2 + \left(\kappa_{o1}^2 - \kappa_{e1}^2\right)\kappa_2 < 0. \tag{11}$$

It is noted that in order to observe a typical CRIT (CRIA), i.e., there is a narrow peak (dip) in the background of a broad dip, it is also required that the quality factor of μR_2 is much larger than that of μR_1, i.e., $\kappa_2 \ll \kappa_{e_1} + \kappa_{o1}$. Defining $D > 0$ ($D < 0$) as CRIT (CRIA) grasps its basic meaning. A discussion about conditions to observe CRIT and CRIA is also given in a very different language in Ref. [34].

IV. TRANSITION BETWEEN CRIT AND CRIA BY CHANGING COUPLING STRENGTHS

How will the shape of the transmission T change as the coupling strength κ_{e1} increases between μR_1 and the fiber taper? The answer is meaningful as it tells what will be observed in experiment when the fiber taper is moved towards μR_1. According to Eqs. (10) and (11), the system is in the CRIT phase for $\kappa_{e1} < \kappa_{e1c}$, with

$$\kappa_{e1c} = \sqrt{\kappa_{o1}^2 + \kappa_{o1}g^2/\kappa_2}, \tag{12}$$

and the system is in the CRIA phase for $\kappa_{e1} > \kappa_{e1c}$. The result predicts that when we fix the gap between the two microresonators and move the fiber taper towards μR_1 from faraway, i.e., increasing κ_{e1} from zero, CRIT will be observed first and then a transition from CRIT to CRIA will happen when the coupling strength κ_{e1} between the fiber taper and μR_1 becomes equal to κ_{e1c}. It is noted that in a real experiment, a transition from CRIT to CRIA may not happen as κ_{e1} may always be smaller than κ_{e1c} no matter how close the fiber taper and μR_1 are.

It is also meaningful to know how the shape of the transmission T will change as the coupling strength g changes between μR_1 and μR_2, which can be tuned in experiment by changing the gap between μR_1 and μR_2. The answer depends on the coupling condition between the fiber taper and μR_1. When the fiber taper and μR_1 are in the overcoupling, i.e., $\kappa_{e1} > \kappa_{o1}$, according to Eqs. (10) and (11) the system is in the CRIA phase for $g < g_c$, with

$$g_c = \sqrt{\left(\kappa_{e1}^2 - \kappa_{o1}^2\right)\kappa_2/\kappa_{o1}}, \tag{13}$$

and the system is in the CRIT phase for $g > g_c$. The result predicts that when we fix the fiber taper and μR_1 in the

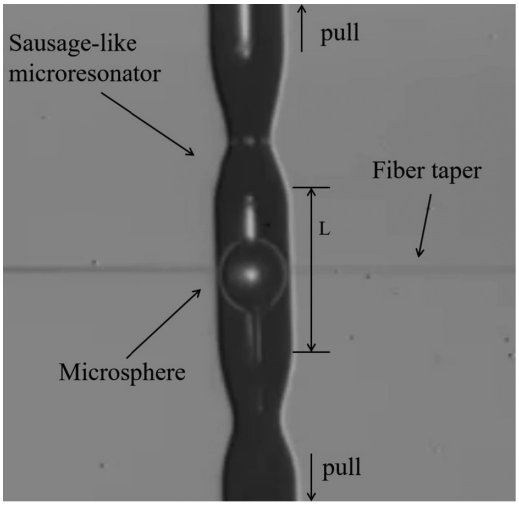

FIG. 2. A micrograph of a SLM and a microsphere. The fiber taper is placed under the SLM and the microsphere is placed above the SLM. The diameter of the microsphere is about 120 μm. The resonant frequency of the SLM can be adjusted by pulling its two ends.

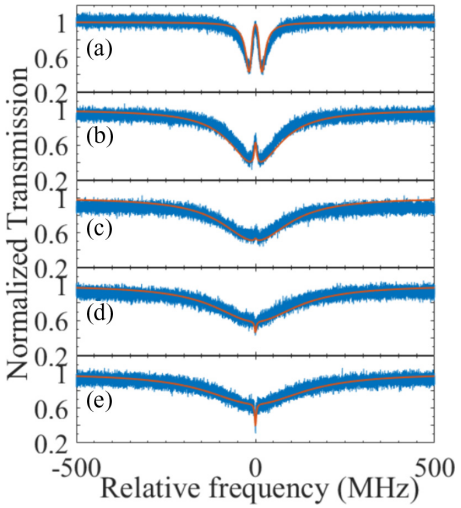

FIG. 3. Observation of the transition from CRIT to CRIA. From (a) to (e), the coupling strength κ_{e1} between the fiber taper and the SLM is increased. The red lines are the theoretical results with the parameters $\kappa_{o1} = 2\pi \times 15.80$ MHz, $g = 2\pi \times 17.90$ MHz, $\kappa_2 = 2\pi \times 0.50$ MHz, $\delta_{12} = 0$, and (a) $\kappa_{e1} = 2\pi \times 3.40$ MHz, (b) $\kappa_{e1} = 2\pi \times 74.50$ MHz, (c) $\kappa_{e1} = 2\pi \times 100.10$ MHz, (d) $\kappa_{e1} = 2\pi \times 125.30$ MHz, and (e) $\kappa_{e1} = 2\pi \times 150.20$ MHz.

overcoupling and move μR_2 towards μR_1 from faraway, i.e., increasing g from zero, CRIA will be observed first and then a transition from CRIA to CRIT will happen when the coupling strength g between μR_2 and μR_1 becomes equal to g_c. It is also noted that in a real experiment, a transition from CRIA to CRIT may not happen as g may always be smaller than g_c no matter how close μR_2 and μR_1 are.

The shape of the transmission T will change in a different manner as the coupling strength g changes when the fiber taper and μR_1 are in the undercoupling or critical coupling. When the fiber taper and μR_1 are in the undercoupling or critical coupling, i.e., $\kappa_{e1} \leqslant \kappa_{o1}$, the system is in the CRIT phase for all g according to Eq. (10). Therefore, CRIT can always be observed as we increase g from zero, but the transmission at the resonance input, i.e., $T|_{\delta_{12}=0,\Delta\omega=0}$, will increase as g increases, according to Eq. (6). The result predicts that when we fix the fiber taper and μR_1 in the undercoupling or critical coupling and move μR_2 towards μR_1 from faraway, CRIT will always be observed and the height of the peak in CRIT will increase as μR_2 is moved closer to μR_1.

V. EXPERIMENTAL RESULTS ON TRANSITIONS BETWEEN CRIT AND CRIA

The experimental setup is shown in Fig. 2, where the SLM has a coupling with the fiber taper [35], and the microsphere has a coupling with the SLM but has no coupling with the fiber taper. The experimental setup is the same as the theoretical setup, where the SLM is corresponding to μR_1 and the microsphere is corresponding to μR_2. The fiber taper is made by using a hydrogen flame to heat a single-mode fiber and, at the same time, stretching it from two sides by a motorized translational stage. The prepared fiber taper is very fragile as its waist diameter is about 2 μm. Some UV glue is used to fix the fiber taper on a U-shaped frame so that we can move the fiber taper by moving the U-shaped frame. The SLM and the microsphere are both made from a single-mode optical fiber using a similar method [27,35]. To prepare them, a single-mode fiber of about 10 cm is placed vertically with a small weight attached to its lower end. A CO_2 laser is used to heat the fiber. The heated part of the fiber will become thinner and thinner due to the gravity so that we can make a thin tip at the lower end of the fiber by moving it. A microsphere can be made by heating the end of the tip using the CO_2 laser. The SLM is made by heating two separate parts of the fiber; the heated parts, due to the gravity, will be thinner than the unheated part, as shown in Fig. 2.

In the experiments, the fiber taper, microsphere, and SLM are attached to independent three-dimensional translation stages with a resolution of 20 nm (MAX312D, Thorlabs), so that we can control the gap between the fiber taper and the SLM, and the the gap between the microsphere and the SLM. The transmission spectra of the system are obtained by using a tunable laser. Laser light is coupled into one port of the fiber taper, and the output from the other port is measured by a photoreceiver to obtain the transmission spectra. The experiments are done in the 1550 nm band. Three parameters that appeared in the theoretical model, i.e., δ_{12}, g, and κ_{e1}, can be adjusted in our experiments. The parameter δ_{12} is the angular frequency detuning between the SLM and the microsphere, which can be adjusted by pulling the SLM from its two ends [27]. The parameter g is the coupling strength between the microsphere and the SLM, which can be increased by moving the microsphere close to the SLM. The parameter κ_{e1} is the coupling strength between the fiber taper and the SLM, which can be increased by moving the fiber taper close to the SLM.

Figure 3 demonstrates how CRIT and CRIA are affected by the coupling strength κ_{e1} between the fiber taper and the SLM. It shows the experimental results with a pair of resonant WGMs when the gap between the microsphere and the SLM

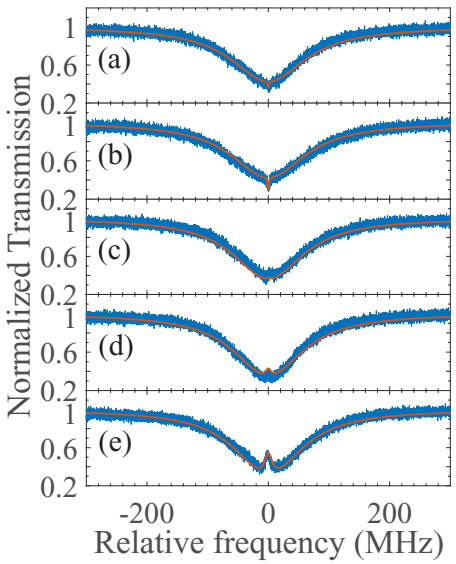

FIG. 4. Observation of the transition from CRIA to CRIT when the fiber taper and the SLM are in the overcoupling. From (a) to (e), the coupling strength g between the microsphere and the SLM is increased. The red lines are the theoretical results with the parameters $\kappa_{o1} = 2\pi \times 12.95$ MHz, $\kappa_{e1} = 2\pi \times 61.69$ MHz, $\kappa_2 = 2\pi \times 1.09$ MHz, $\delta_{12} = 0$, and (a) $g = 2\pi \times 1.60$ MHz, (b) $g = 2\pi \times 2.30$ MHz, (c) $g = 2\pi \times 16.30$ MHz, (d) $g = 2\pi \times 17.60$ MHz, and (e) $g = 2\pi \times 20.90$ MHz.

is fixed. According to the theory, when the fiber taper is moved towards the SLM, CRIT will be observed first and then a transition from CRIT to CRIA may happen. In Figs. 3(a) to 3(e), the fiber taper is moved closer and closer to the SLM, which means an increasing of the coupling strength κ_{e1}. As predicted by the theory, we first observe CRIT, and when we

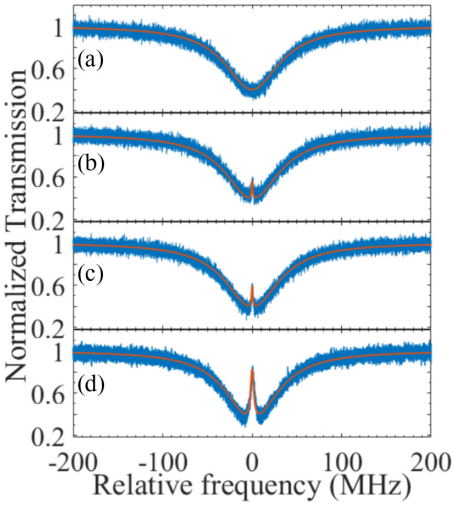

FIG. 5. Observation of the influence of g on CRIT when the fiber taper and the SLM are in the undercoupling. From (a) to (d), the coupling strength g between the microsphere and the SLM is increased. The red lines are the theoretical results with the parameters $\kappa_{o1} = 2\pi \times 30.10$ MHz, $\kappa_{e1} = 2\pi \times 6.80$ MHz, $\kappa_2 = 2\pi \times 0.50$ MHz, $\delta_{12} = 0$, and (a) $g = 0$ MHz, (b) $g = 2\pi \times 3.00$ MHz, (c) $g = 2\pi \times 3.40$ MHz, and (d) $g = 2\pi \times 7.50$ MHz.

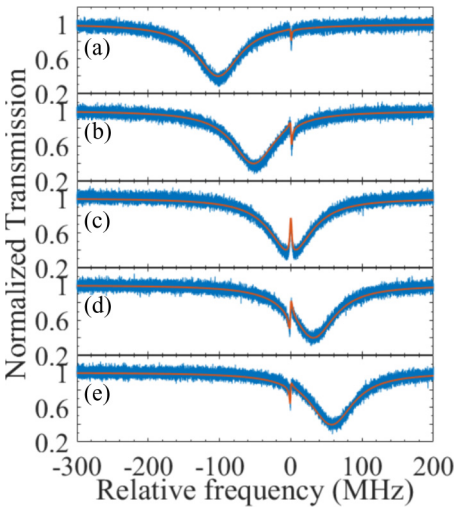

FIG. 6. Observation of the transition between CRIT and Fano resonance. From (a) to (e), the resonant frequency of the SLM is increased. The red lines are the theoretical results with the parameters $\kappa_{o1} = 2\pi \times 30.10$ MHz, $\kappa_{e1} = 2\pi \times 6.80$ MHz, $\kappa_2 = 2\pi \times 0.50$ MHz, $g = 2\pi \times 6.20$ MHz, and (a) $\delta_{12} = -2\pi \times 101.50$ MHz, (b) $\delta_{12} = -2\pi \times 51.50$ MHz, (c) $\delta_{12} = 0$, (d) $\delta_{12} = 2\pi \times 30.50$ MHz, and (e) $\delta_{12} = 2\pi \times 56.50$ MHz.

move the fiber taper closer to the SLM, a transition from CRIT to CRIA is observed. In Fig. 3, it can be found that the width of the peak in CRIT is much larger than the width of the dip in CRIA, which is interesting and may be used in sensing.

Figures 4 and 5 show how CRIT and CRIA are affected by the coupling strength g between the microsphere and the SLM. Figure 4 shows the experimental results with a pair of resonant WGMs when the fiber taper and the SLM are fixed in the overcoupling, i.e., $\kappa_{o1} < \kappa_{e1}$, where, from Figs. 4(a) to 4(e), the coupling strength g between the SLM and the microsphere

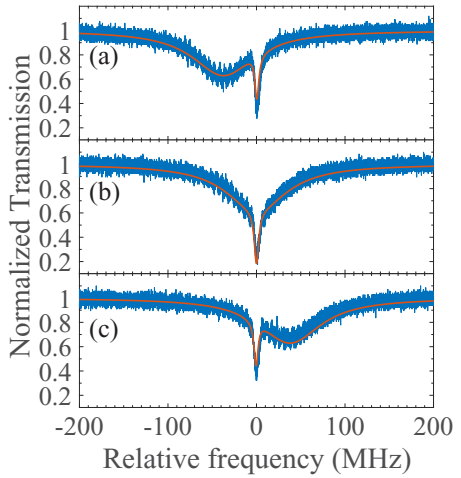

FIG. 7. Observation of the transition between CRIA and Fano resonance. From (a) to (c), the resonant frequency of the SLM is increased. The red lines are the theoretical results with the parameters $\kappa_{o1} = 2\pi \times 4.40$ MHz, $\kappa_{e1} = 2\pi \times 38.51$ MHz, $\kappa_2 = 2\pi \times 2.36$ MHz, $g = 2\pi \times 5.10$ MHz, and (a) $\delta_{12} = -2\pi \times 36.87$ MHz, (b) $\delta_{12} = 0$, and (c) $\delta_{12} = 2\pi \times 37.50$ MHz.

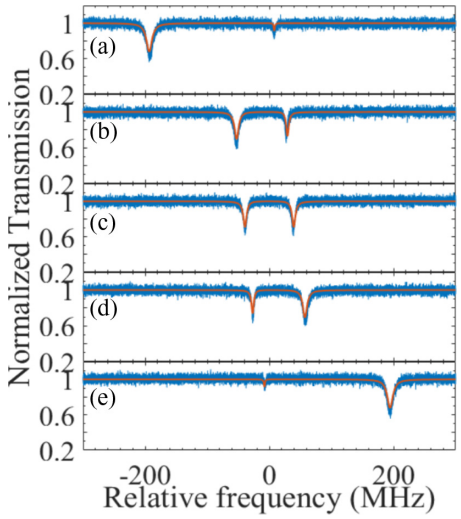

FIG. 8. Observation of the ATS phenomenon. From (a) to (e), the resonant frequency of the SLM is increased. The red lines are the theoretical fittings with the parameters $\kappa_{o1} = 2\pi \times 5.10$ MHz, $\kappa_{e1} = 2\pi \times 0.50$ MHz, $\kappa_2 = 2\pi \times 0.67$ MHz, $g = 2\pi \times 39.20$ MHz, and (a) $\delta_{12} = -2\pi \times 185.50$ MHz, (b) $\delta_{12} = -2\pi \times 24.40$ MHz, (c) $\delta_{12} = 0$, (d) $\delta_{12} = 2\pi \times 30.50$ MHz, and (e) $\delta_{12} = 2\pi \times 186.50$ MHz.

is increased. As predicted by the theory, CRIA is observed at the beginning and then a transition from CRIA to CRIT is observed. Figure 5 shows the experimental results with a pair of resonant WGMs when the fiber taper and the SLM are fixed in the undercoupling, i.e., $\kappa_{o1} > \kappa_{e1}$, and move the microsphere towards the SLM from faraway. In Figs. 5(a)–5(d), the microsphere is moved closer and closer to the SLM, which means an increasing of the coupling strength g between the SLM and the microsphere. It can be found that as the coupling strength g increases, the height of the central peak of the CRIT becomes higher and higher, which proves the theoretical prediction.

We also investigate how CRIT and CRIA are affected by the angular frequency detuning δ_{12} between the SLM and the microsphere. The results are shown in Figs. 6 to 8. In these experiments, we pull the SLM from its two ends, which increases the angular frequency of the mode of the SLM. The angular frequency of the mode of the microsphere does not change during pulling the SLM, therefore the angular frequency detuning δ_{12} will increase when the SLM is pulled from its two ends. Figure 6 shows the transition between CRIT and Fano resonance by tuning the angular frequency detuning δ_{12}, where, from Figs. 6(a) to 6(e), the angular frequency detuning δ_{12} is increased, and the fiber taper and the SLM are in the undercoupling. In the experiment, the quality factor of the mode of the SLM is much smaller than that of the mode of the microsphere, i.e., $\kappa_{o1} + \kappa_{e1} \gg \kappa_2$, which is important to the observation of the typical CRIT in the middle of Fig. 6. Figure 7 shows the transition between CRIA and Fano resonance by tuning the angular frequency detuning δ_{12}, where the fiber taper and the SLM are in the overcoupling. In the experiment, the quality factor of the mode of the SLM is much smaller than that of the mode of the microsphere, which is also important to the observation of the typical CRIA in the middle of Fig. 7. It can be found that Fano resonance transmitted from CRIA has no sharp peak, while Fano resonance transmitted from CRIT has a sharp peak. We note that for the experiments shown in Figs. 6 and 7, the coupling strength g between the SLM and the microsphere is much smaller than the decay rate of the mode of the SLM, i.e., $g \ll \kappa_{o1} + \kappa_{e1}$. When the coupling strength g is much larger than the decay rate of the mode of the SLM, the phenomena will be different as shown in Fig. 8. Compared to Fig. 6, it does not show a typical CRIT when $\delta_{12} = 0$ in the middle of Fig. 8, but shows the ATS phenomenon. This is because the coupling strength g between the SLM and the microsphere is much larger than the decay rate of the mode of the SLM [12].

VI. SUMMARY

In summary, we investigate CRIT and CRIA in two coupled WGM microresonators theoretically and experimentally. We first give the theoretical normalized transmission of the coupled system and then focus on the cases in which the two microresonators have the same resonant frequency. By considering the influence of the coupling between two microresonators on the transmission at the resonance input, we give the conditions to observe CRIT and CRIA and predict that a transition between them can be observed by changing the coupling strength between the two microresonators or the coupling strength between the fiber taper and the first microresonator. We experimentally measure the transmission spectra of a SLM coupled with a microsphere and demonstrate the predicted transitions between CRIT and CRIA. Our experimental results also show how CRIT and CRIA are influenced by the frequency detuning between the SLM and the microsphere. The theoretical results fit well with the experimental results. The obtained results give some guidelines to observe CRIT and CRIA, and have potential applications such as slow-light generation [10] and sensing [36–38].

ACKNOWLEDGMENTS

This work was supported by the National Natural Science Foundation of China (Grant No. 11674059).

[1] M. Fleischhauer, A. Imamoglu, and J. P. Marangos, Electromagnetically induced transparency: Optics in coherent media, Rev. Mod. Phys. **77**, 633 (2005).

[2] Y. C. Liu, B. B. Li, and Y. F. Xiao, Electromagnetically induced transparency in optical microcavities, Nanophotonics **6**, 789 (2017).

[3] Q. Xu, S. Sandhu, M. L. Povinelli, J. Shakya, S. Fan, and M. Lipson, Experimental Realization of an On-Chip All-Optical Analogue to Electromagnetically Induced Transparency, Phys. Rev. Lett. **96**, 123901 (2006).

[4] Y. Wang, K. Zhang, S. Zhou, Y. H. Wu, M. B. Chi, and P. Hao, Coupled-mode induced transparency in a bottle whispering-gallery-mode resonator, Opt. Lett. **41**, 1825 (2016).

[5] Y. Yang, S. Saurabh, J. Ward, and S. N. Chormaic, Coupled-mode-induced transparency in aerostatically tuned microbubble whispering-gallery resonators, Opt. Lett. **40**, 1834 (2015).

[6] X. Y. Jin, Y. C. Dong, and K. Y. Wang, Stable controlling of electromagnetically induced transparency-like in a single quasi-cylindrical microresonator, Opt. Express **24**, 29773 (2016).

[7] Y. L. Zheng, J. F. Yang, Z. H. Shen, J. J. Cao, X. F. Chen, X. G. Liang, and W. J. Wan, Optically induced transparency in a micro-cavity, Light: Sci. Appl. **5**, e16072 (2016).

[8] X. Liu, Q. Lu, L. Fu, X. Chen, X. Wu, and S. Xie, Coupled-mode induced transparency via Ohmic heating in a single polydimethylsiloxane-coated microbubble resonator, Opt. Express **28**, 10705 (2020).

[9] A. Naweed, G. Farca, S. I. Shopova, and A. T. Rosenberger, Induced transparency and absorption in coupled whispering-gallery microresonators, Phys. Rev. A **71**, 043804 (2005).

[10] K. Totsuka, N. Kobayashi, and M. Tomita, Slow Light in Coupled-Resonator-Induced Transparency, Phys. Rev. Lett. **98**, 213904 (2007).

[11] C. Zheng, X. S. Jiang, S. Y. Hua, L. Chang, G. Y. Li, H. B. Fan, and M. Xiao, Controllable optical analog to electromagnetically induced transparency in coupled high-Q microtoroid cavities, Opt. Express **20**, 18319 (2012).

[12] B. Peng, Ş. K. Özdemir, W. J. Chen, F. Nori, and L. Yang, What is and what is not electromagnetically induced transparency in whispering-gallery microcavities, Nat. Commun. **5**, 5082 (2014).

[13] W. Yoshiki, Y. Honda, T. Tetsumoto, K. Furusawa, N. Sekine, and T. Tanabe, All-optical tunable buffering with coupled ultra-high Q whispering gallery mode microcavities, Sci. Rep. **7**, 10688 (2017).

[14] S. Weis, R. Rivière, S. Deléglise, E. Gavartin, O. Arcizet, A. Schliesser, and T. J. Kippenberg, Optomechanically induced transparency, Science **330**, 1520 (2010).

[15] Z. Shen, C. H. Dong, Y. Chen, Y. F. Xiao, F. W. Sun, and G. C. Guo, Compensation of the Kerr effect for transient optomechanically induced transparency in a silica microsphere, Opt. Lett. **41**, 1249 (2016).

[16] C. H. Dong, Z. Shen, C. L. Zou, Y. L. Zhang, W. Fu, and G. C. Guo, Brillouin-scattering-induced transparency and non-reciprocal light storage, Nat. Commun. **6**, 6193 (2015).

[17] H. Xiong and Y. Wu, Fundamentals and applications of optomechanically induced transparency, Appl. Phys. Rev. **5**, 031305 (2018).

[18] L. Ge, L. Feng, and H. G. L. Schwefel, Optical microcavities: New understandings and developments, Photon. Res. **5**, OM1 (2017).

[19] Q. H. Song, Emerging opportunities for ultra-high Q whispering gallery mode microcavities, Sci. China-Phys. Mech. Astron. **62**, 074231 (2019).

[20] S. Wan, R. Niu, Z. Y. Wang, J. L. Peng, M. Li, J. Li, G. C. Guo, C. L. Zou, and C. H. Dong, Frequency stabilization and tuning of breathing soliton in Si3N4 microresonators, Photon. Res. **8**, 1342 (2020).

[21] D. D. Smith, H. Chang, K. A. Fuller, A. T. Rosenberger, and R. W. Boyd, Coupled-resonator-induced transparency, Phys. Rev. A **69**, 063804 (2004).

[22] T. Wang, Y. Q. Hu, C. G. Du, and G. L. Long, Multiple EIT and EIA in optical microresonators, Opt. Express **27**, 7344 (2019).

[23] C. Wang, X. Jiang, G. Zhao, M. Zhang, C. W. Hsu, B. Peng, A. D. Stone, L. Jiang, and L. Yang, Electromagnetically induced transparency at a chiral exceptional point, Nat. Phys. **16**, 334 (2020).

[24] Z. Chen, Y. Zhou, and J. T. Shen, Photon antibunching and bunching in a ring-resonator waveguide quantum electrodynamics system, Opt. Lett. **41**, 3313 (2016).

[25] Z. Chen, Y. Zhou, and J. T. Shen, Dissipation-induced photonic-correlation transition in waveguide-QED systems, Phys. Rev. A **96**, 053805 (2017).

[26] Y. Zhou, Z. Chen, and J. T. Shen, Single-photon superradiance in waveguide-quantum-electrodynamical systems with whispering-gallery-mode resonators, Phys. Rev. A **101**, 043831 (2020).

[27] M. Y. Ye, M. X. Shen, and X. M. Lin, Transmission spectra of sausage-like microresonators, Opt. Express **23**, 25846 (2015).

[28] B. B. Li, Y. F. Xiao, C. L. Zou, X. F. Jiang, Y. C. Liu, F. W. Sun, Y. Li, and Q. H. Gong, Experimental controlling of Fano resonance in indirectly coupled whispering-gallery microresonators, Appl. Phys. Lett. **100**, 021108 (2012).

[29] P. F. Chang, B. T. Cao, L. G. Huang, J. W. Li, Y. Hu, F. Gao, W. D. Zhang, F. Bo, X. Y. Yu, G. Q. Zhang, and J. J. Xu, Polarization-modified Fano line shape spectrum with a single whispering gallery mode, Sci. China-Phys. Mech. Astron. **63**, 214211 (2020).

[30] X. Zhang, Y. Yang, H. Shao, H. Bai, F. Pang, H. Xiao, and T. Wang, Fano resonances in cone-shaped inwall capillary based microsphere resonator, Opt. Express **25**, 615 (2017).

[31] J. Liao, X. Wu, L. Liu, and L. Xu, Fano resonance and improved sensing performance in a spectral-simplified optofluidic microbubble resonator by introducing selective modal losses, Opt. Express **24**, 8574 (2016).

[32] Y. L. Shang, M. Y. Ye, and X. M. Lin, Experimental observation of Fano-like resonance in a whispering-gallery-mode microresonator in aqueous environment, Photon. Res. **5**, 119 (2017).

[33] A. E. Miroshnichenko, S. Flach, and Y. S. Kivshar, Fano resonances in nanoscale structures, Rev. Mod. Phys. **82**, 2257 (2010).

[34] D. D. Smith and H. Chang, Coherence phenomena in coupled optical resonators, J. Mod. Optic. **51**, 2503 (2004).

[35] M. Y. Ye, M. X. Shen, and X. M. Lin, Ringing phenomenon based whispering-gallery-mode sensing, Sci. Rep. **6**, 19597 (2016).

[36] S.-J. Tang, B.-B. Li, and Y.-F. Xiao, Optical sensing with whispering-gallery microcavities, Physics **48**, 137 (2019).

[37] G. C. Righini and S. Soria, Biosensing by WGM microspherical resonators, Sensors **16**, 905 (2016).

[38] X. Jiang, A. J. Qavi, S. H. Huang, and L. Yang, Whispering gallery microsensors: A review, arXiv:1805.00062.